J|A|C|S
A R T I C L E S

^{89}Y and ^{13}C NMR Cluster and Carbon Cage Studies of an Yttrium Metallofullerene Family, Y$_3$N@C$_{2n}$ (n = 40−43)

Wujun Fu, Liaosa Xu, Hugo Azurmendi, Jiechao Ge, Tim Fuhrer, Tianming Zuo, Jonathan Reid, Chunying Shu, Kim Harich, and Harry C. Dorn*

Department of Chemistry, Virginia Polytechnic Institute and State University, Blacksburg, Virginia 24060

Received March 23, 2009; E-mail: hdorn@vt.edu

Abstract: The members of a new family of yttrium trimetallic nitride-templated (TNT) endohedral metallofullerenes (EMFs), Y$_3$N@C$_{2n}$ (n = 40−43), have been synthesized and purified. On the basis of experimental and computational ^{13}C NMR studies, we propose cage structures for Y$_3$N@I_h-C$_{80}$ (IPR allowed), Y$_3$N@D_{5h}-C$_{80}$ (IPR allowed), Y$_3$N@C_s-C$_{82}$ (non-IPR), Y$_3$N@C_s-C$_{84}$ (non-IPR), and Y$_3$N@D_3-C$_{86}$ (IPR allowed). A significant result is the limited number of isomers found for each carbon cage. For example, there are 24 isolated pentagon rule (IPR) and 51 568 non-IPR structures possible for the C$_{84}$ cage, but only one major isomer of Y$_3$N@C_s-C$_{84}$ was found. The current study confirms the unique role of the trimetallic nitride (M$_3$N)$^{6+}$ cluster template in the Krätschmer−Huffman electric-arc process for fullerene cage size and high symmetry isomer selectivity. This study reports the first ^{89}Y NMR results for Y$_3$N@I_h-C$_{80}$, Y$_3$N@C_s(51365)-C$_{84}$, and Y$_3$N@D_3(19)-C$_{86}$, which reveal a progression from isotropic to restricted (Y$_3$N)$^{6+}$ cluster motional processes. Even more surprising is the sensitivity of the ^{89}Y NMR chemical shift parameter to subtle changes in the electronic environment at each yttrium nuclide in the (Y$_3$N)$^{6+}$ cluster (more than 200 ppm for these EMFs). This ^{89}Y NMR study suggests that ^{89}Y NMR will evolve as a powerful tool for cluster motional studies of EMFs.

Introduction

There is increasing interest in trimetallic nitride-templated (TNT) endohedral metallofullerenes (EMFs) M$_3$N@C$_{2n}$ (n = 34−50) because of their interesting electronic and structural properties,[1,2] In comparison with empty-cage fullerenes (C$_{60}$, C$_{70}$, and C$_{84}$), the higher stability of the TNT EMFs has enabled several chemical-separation approaches based on the corresponding lower chemical reactivity of the M$_3$N@C$_{2n}$ families.[3−5] Conversely, the TNT EMFs still exhibit sufficient chemical reactivity for a variety of different chemical reactions, including Bingel−Hirsch,[6−8] Prato,[9−13] and free-radical reactions.[14] In addition, potential applications of TNT EMFs are emerging in diverse areas, including use as photovoltaic devices[15,16] and MRI contrast agents.[17−30]

It is now clear that the size of the trimetallic cluster (M$_3$N)$^{6+}$ plays an important role in dictating how the TNT EMF isomer

(1) Shinohara, H. *Rep. Prog. Phys.* **2000**, *63*, 843−892.
(2) Akasaka, T.; Nagase, S. *Endofullerenes: A New Family of Carbon Cluster*; Kluwer Academic Publishers: Dordrecht, The Netherlands, 2002.
(3) Ge, Z.; Duchamp, J. C.; Cai, T.; Gibson, H. W.; Dorn, H. C. *J. Am. Chem. Soc.* **2005**, *127*, 16292−16298.
(4) Stevenson, S.; Harich, K.; Yu, H.; Stephen, R. R.; Heaps, D.; Coumbe, C.; Phillips, J. P. *J. Am. Chem. Soc.* **2006**, *128*, 8829−8835.
(5) Angeli, C. D.; Cai, T.; Duchamp, J. C.; Reid, J. E.; Singer, E. S.; Gibson, H. W.; Dorn, H. C. *Chem. Mater.* **2008**, *20*, 4993−4997.
(6) Lukoyanova, O.; Cardona, C. M.; Rivera, J.; Lugo-Morales, L. Z.; Chancellor, C. J.; Olmstead, M. M.; Rodríguez-Fortea, A.; Poblet, J. M.; Balch, A. L.; Echegoyen, L. *J. Am. Chem. Soc.* **2007**, *129*, 10423−10430.
(7) Cai, T.; Xu, L.; Shu, C.; Champion, H. A.; Reid, J. E.; Anklin, C.; Anderson, M. R.; Gibson, H. W.; Dorn, H. C. *J. Am. Chem. Soc.* **2008**, *130*, 2136−2137.
(8) Pinzón, J. R.; Cardona, C. M.; Herranz, M. A.; Plonska-Brzezinska, M. E.; Palkar, A.; Athans, A. J.; Martín, N.; Rodríguez-Fortea, A.; Poblet, J. M.; Bottari, G.; Torres, T.; Gayathri, S. S.; Guldi, D. M.; Echegoyen, L. *Chem.−Eur. J.* **2009**, *15*, 864−877.
(9) Cardona, C. M.; Kitaygorodskiy, A.; Echegoyen, L. *J. Am. Chem. Soc.* **2005**, *127*, 10448−10453.
(10) Cai, T.; Ge, Z.; Lezzi, E. B.; Glass, T. E.; Gibson, H. W.; Dorn, H. C. *Chem. Commun.* **2005**, 3594−3596.
(11) Echegoyen, L.; Chancellor, C. J.; Cardona, C. M.; Elliott, B.; Rivera, J.; Olmstead, M. M.; Balch, A. L. *Chem. Commun.* **2006**, 2653−2655.
(12) Cai, T.; Slebodnick, C.; Xu, L.; Glass, T. E.; Chancellor, C.; Fettinger, J. C.; Olmstead, M. M.; Balch, A. L.; Gibson, H. W.; Dorn, H. C. *J. Am. Chem. Soc.* **2006**, *128*, 6486−6492.
(13) Cai, T.; Xu, L.; Gibson, H. W.; Dorn, H. C.; Chancellor, C.; Olmstead, M. M.; Balch, A. L. *J. Am. Chem. Soc.* **2007**, *129*, 10795−10800.
(14) Shu, C.; Cai, T.; Xu, L.; Zuo, T.; Reid, J. E.; Harich, K.; Dorn, H. C.; Gibson, H. W. *J. Am. Chem. Soc.* **2007**, *129*, 15710−15717.
(15) Thompson, B. C.; Fréchet, J. M. J. *Angew. Chem., Int. Ed.* **2008**, *47*, 58−77.
(16) Ross, R. B.; Cardona, C. M.; Guldi, D. M.; Sankaranarayanan, S. G.; Reese, M. O.; Kopidakis, N.; Peet, J.; Walker, B.; Bazan, G. C.; Keuren, E. V.; Holloway, B. C.; Drees, M. *Nat. Mater.* **2009**, *8*, 208−212.
(17) Zhang, S. R.; Sun, D. Y.; Li, X. Y.; Pei, F. K.; Liu, S. Y. *Fullerene Sci. Technol.* **1997**, *5*, 1635−1643.
(18) Wilson, L. J.; Cagle, D. W.; Thrash, T. P.; Kennel, S. J.; Mirzadeh, S.; Alford, J. M.; Ehrhardt, G. J. *Coord. Chem. Rev.* **1999**, *192*, 199−207.
(19) Wilson, L. J. *Electrochem. Soc. Interface* **1999**, No. 4, 24−28.
(20) Mikawa, M.; Kato, H.; Okumura, M.; Narataki, M.; Kanazawa, Y.; Miwa, N.; Shinohara, H. *Bioconjugate Chem.* **2001**, *12*, 510−514.
(21) Iezzi, E. B.; Duchamp, J. C.; Fletcher, K. R.; Glass, T. E.; Dorn, H. C. *Nano Lett.* **2002**, *2*, 1187−1190.
(22) Okumura, M.; Mikawa, M.; Yokawa, T.; Kanazawa, Y.; Kato, H.; Shinohara, H. *Acad. Radiol.* **2002**, *9*, S495−S497.
(23) Kato, H.; Kanazawa, Y.; Okuura, M.; Taninaka, A.; Yokawa, T.; Shinohara, H. *J. Am. Chem. Soc.* **2003**, *125*, 4391−4397.

formed. To illustrate, the first protypical scandium member of the TNT EMF family, $Sc_3N@C_{80}$, was determined to be $Sc_3N@I_h$-C_{80}, with stabilization of the icosahedral I_h cage by transfer of six electrons to the fullerene cage $(C_{80})^{6-}$. However, it was later discovered by ^{13}C NMR analysis[31] that a second isomer, $Sc_3N@D_{5h}$-C_{80}, was present in the Krätschmer−Huffman reaction mixture. This isomer was later isolated and structurally characterized by single-crystal X-ray diffraction analysis.[32] With the smaller scandium ions present in the trimetallic cluster $(Sc_3N)^{6+}$, a smaller non-isolated pentagon rule (non-IPR) structure, $Sc_3N@D_3$-C_{68}, was also first identified by ^{13}C NMR and later structurally characterized by single-crystal X-ray diffraction analysis.[33,34] A second cage containing fewer than 80 carbons, $Sc_3N@D_{3h}$-C_{78} was also characterized by both ^{13}C NMR and single-crystal X-ray studies.[35] More recently, TNT EMFs with larger lanthanide (Ln) trimetallic clusters $(Ln_3N)^{6+}$ have been produced and characterized in the laboratories of Balch, Dunsch, and Echegoyen, including $Gd_3N@C_{2n}$ ($n = 40−44$),[36,37] $Tm_3N@C_{2n}$ ($n = 39−44$),[38] $Dy_3N@C_{2n}$ ($n = 38−44$),[39] $Tb_3N@C_{2n}$ ($n = 40, 42−44$),[40,41] $Nd_3N@C_{2n}$ ($n = 40−50$),[42,43] $Pr_3N@C_{2n}$ ($n = 40−52$),[43] $Ce_3N@C_{2n}$ ($n = 43−53$),[43] and $La_3N@C_{2n}$ ($n = 43−55$).[44] To illustrate, detailed

single-crystal X-ray structural information has been obtained for mostly the $Ln_3N@C_{80}$ family, such as $Gd_3N@I_h$-C_{80},[45,46] $Dy_3N@I_h$-C_{80},[47] $Lu_3@I_h$-C_{80},[48] $Tm_3N@I_h$-C_{80},[49] $Tm_3N@D_{5h}$-C_{80},[49] $Tb_3N@I_h$-C_{80},[41] and $Tb_3N@D_{5h}$-C_{80},[41] as well as for the larger cages $Gd_3N@C_s(39663)$-C_{82},[50] $Tb_3N@C_s(51365)$-C_{84},[40] $Gd_3N@C_s(51365)$-C_{84},[51] $Tm_3N@C_s(51365)$-C_{84},[51] $Tb_3N@D_3$-C_{86},[41] and $Tb_3N@D_2$-C_{88}.[41] An unusual result of these latter studies is the limited number of isomers observed for a given cage size.

In this paper, we report a ^{89}Y and ^{13}C NMR study of a new family of TNT EMFs represented by the diamagnetic yttrium EMFs $Y_3N@C_{2n}$ ($n = 40−43$). This family is an important contrast to previous studies, since high-resolution ^{13}C NMR studies are usually not feasible for the paramagnetic lanthanide TNT EMFs but the ^{89}Y nuclide provides a new tool for monitoring motional processes of the $(Y_3N)^{6+}$ cluster. Although the ^{89}Y nuclide is 100% abundant, solution ^{89}Y NMR studies have been hampered by the small magnetogyric ratio and corresponding long spin−lattice (T_1) relaxation times for this nuclide. However, Sherry and co-workers[52] have recently pointed out the advantages of using hyperpolarized ^{89}Y for direct imaging in biological systems. Their study also illustrates the importance of dynamic nuclear polarization (DNP) to alleviate sensitivity issues of this small-magnetogyric-ratio nuclide.

In addition, the size of the $(Y_3N)^{6+}$ cluster is intermediate in comparison with the smaller scandium and generally larger lanthanide clusters. This posed the interesting question of whether the trimetallic nitride template Krätschmer−Huffman process would provide fullerene cages analogous to the smaller scandium cages or the larger unique cages observed for the lanthanides (see above). The members of the $Y_3N@C_{2n}$ ($n = 40−43$) family were isolated and purified utilizing chemical separation (Diels−Alder) on a cyclopentadiene-functionalized chromatogram and two-stage high-performance liquid chromatography (HPLC).

Experimental and Computational Methods

Preparation of $Y_3N@C_{2n}$. The samples were prepared in a Krätschmer−Huffman generator by vaporizing composite graphite rods containing a 1.1:1.0:2.1 (w/w/w) mixture of Y_2O_3, graphite powder, and metallic Cu (as the catalyst) in a dynamic flow of He and N_2 (N_2/H_2 flow-rate ratio = 3:100). The resulting soot was then extracted with refluxing toluene in a Soxhlet extractor for 24 h to obtain the soluble extract for further purification.

Purification of $Y_3N@C_{2n}$. Cyclopentadiene-functionalized Merrifield peptide resin (CPDE-MPR) (45 g) was synthesized as previously described[3] and packed in a glass column (22 × 450 mm). The soot extract was applied to the glass column and flushed using toluene (20 mL/h). The eluent was further separated by two-

(24) Bolskar, R. D.; Benedetto, A. F.; Husebo, L. O.; Price, R. E.; Jackson, E. F.; Wallace, S.; Wilson, L. J.; Alford, J. M. *J. Am. Chem. Soc.* **2003**, *125*, 5471–5478.

(25) Fatouros, P. P.; Corwin, F. D.; Chen, Z. J.; Broaddus, W. C.; Tatum, J. L.; Kettenmann, B.; Ge, Z.; Gibson, H. W.; Russ, J. L.; Leonard, A. P.; Duchamp, J. C.; Dorn, H. C. *Radiology* **2006**, *240*, 756–764.

(26) Zhang, E.; Shu, C.; Feng, L.; Wang, C. *J. Phys. Chem. B* **2007**, *111*, 14223–14226.

(27) Sitharaman, B.; Wilson, L. J. *J. Biomed. Nanotechnol.* **2007**, *3*, 342–352.

(28) Chaur, M. N.; Melin, F.; Athans, A. J.; Elliott, B.; Walker, K.; Holloway, B. C.; Echegoyen, L. *Chem. Commun.* **2008**, 2665–2667.

(29) Shu, C.; Wang, C.; Zhang, J.; Gibson, H. W.; Dorn, H. C.; Corwin, F. D.; Fatouros, P. P.; Dennis, T. J. S. *Chem. Mater.* **2008**, *20*, 2106–2109.

(30) Shu, C.; Ma, X.; Zhang, J.; Corwin, F. D.; Sim, J. H.; Zhang, E. Y.; Dorn, H. C.; Gibson, H. W.; Fatouros, P. P.; Wang, C. R.; Fang, X. H. *Bioconjugate Chem.* **2008**, *19*, 651–655.

(31) Duchamp, J. C.; Demortier, A.; Fletcher, K. R.; Dorn, D.; Iezzi, E. B.; Glass, T.; Dorn, H. C. *Chem. Phys. Lett.* **2003**, *375*, 655–659.

(32) Cai, T.; Xu, L.; Anderson, M. R.; Ge, Z.; Zuo, T.; Wang, X.; Olmstead, M. M.; Balch, A. L.; Gibson, H. W.; Dorn, H. C. *J. Am. Chem. Soc.* **2006**, *128*, 8581–8589.

(33) Stevenson, S.; Fowler, P. W.; Heine, T.; Duchamp, J. C.; Rice, G.; Glass, T.; Harich, K.; Hajdu, E.; Bible, R.; Dorn, H. C. *Nature* **2000**, *408*, 427–428.

(34) Olmstead, M. M.; Lee, H. M.; Duchamp, J. C.; Stevenson, S.; Marciu, D.; Dorn, H. C.; Balch, A. L. *Angew. Chem., Int. Ed.* **2003**, *42*, 900–903.

(35) Olmstead, M. M.; De Bettencourt-Dias, A.; Duchamp, J. C.; Stevenson, S.; Marciu, D.; Dorn, H. C.; Balch, A. L. *Angew. Chem., Int. Ed.* **2001**, *40*, 1223–1225.

(36) Krause, M.; Dunsch, L. *Angew. Chem., Int. Ed.* **2005**, *44*, 1557–1560.

(37) Chaur, M. N.; Melin, F.; Elliott, B.; Athans, A. J.; Walker, K.; Holloway, B. C.; Echegoyen, L. *J. Am. Chem. Soc.* **2007**, *129*, 14826–14829.

(38) Krause, M.; Wong, J.; Dunsch, L. *Chem.−Eur. J.* **2005**, *11*, 706–711.

(39) Yang, S.; Dunsch, L. *J. Phys. Chem. B* **2005**, *109*, 12320–12328.

(40) Beavers, C. M.; Zuo, T.; Duchamp, J. C.; Harich, K.; Dorn, H. C.; Olmstead, M. M.; Balch, A. L. *J. Am. Chem. Soc.* **2006**, *128*, 11352–11353.

(41) Zuo, T.; Beavers, C. M.; Duchamp, J. C.; Campbell, A.; Dorn, H. C.; Olmstead, M. M.; Balch, A. L. *J. Am. Chem. Soc.* **2007**, *129*, 2035–2043.

(42) Melin, F.; Chaur, M. N.; Engmann, S.; Elliott, B.; Kumbhar, A.; Athans, A. J.; Echegoyen, L. *Angew. Chem., Int. Ed.* **2007**, *46*, 9032–9035.

(43) Chaur, M. N.; Melin, F.; Elliott, B.; Kumbhar, A.; Athans, A. J.; Echegoyen, L. *Chem.−Eur. J.* **2008**, *14*, 4594–4599.

(44) Chaur, M. N.; Melin, F.; Ashby, J.; Elliott, B.; Kumbhar, A.; Rao, A. M.; Echegoyen, L. *Chem.−Eur. J.* **2008**, *14*, 8213–8219.

(45) Stevenson, S.; Phillips, J. P.; Reid, J. E.; Olmstead, M. M.; Rath, S. P.; Balch, A. L. *Chem. Commun.* **2004**, 2814–2815.

(46) Krause, M.; Dunsch, L. *Angew. Chem., Int. Ed.* **2005**, *44*, 1557–1560.

(47) Yang, S.; Troyanov, S. I.; Popov, A. A.; Krause, M.; Dunsch, L. *J. Am. Chem. Soc.* **2006**, *128*, 16733–16739.

(48) Stevenson, S.; Lee, H. M.; Olmstead, M. M.; Kozikowski, C.; Stevenson, P.; Balch, A. L. *Chem.−Eur. J.* **2002**, *8*, 4528–4535.

(49) Zuo, T.; Olmstead, M. M.; Beavers, C. M.; Balch, A. L.; Wang, G.; Yee, G. T.; Shu, C.; Xu, L.; Elliott, B.; Echegoyen, L.; Duchamp, J. C.; Dorn, H. C. *Inorg. Chem.* **2008**, *47*, 5234–5244.

(50) Mercado, B. Q.; Beavers, C. M.; Olmstead, M. M.; Chaur, M. N.; Walker, K.; Holloway, B. C.; Echegoyen, L.; Balch, A. L. *J. Am. Chem. Soc.* **2008**, *130*, 7854–7855.

(51) Zuo, T.; Walker, K.; Olmstead, M. M.; Melin, F.; Holloway, B. C.; Echegoyen, L.; Dorn, H. C.; Chaur, M. N.; Chancellor, C. J.; Beavers, C. M.; Balch, A. L.; Athans, A. J. *Chem. Commun.* **2008**, 1067–1069.

(52) Merritt, M. E.; Harrison, C.; Kovacs, Z.; Kshirsagar, P.; Malloy, C. R.; Sherry, A. D. *J. Am. Chem. Soc.* **2007**, *129*, 12942–12943.
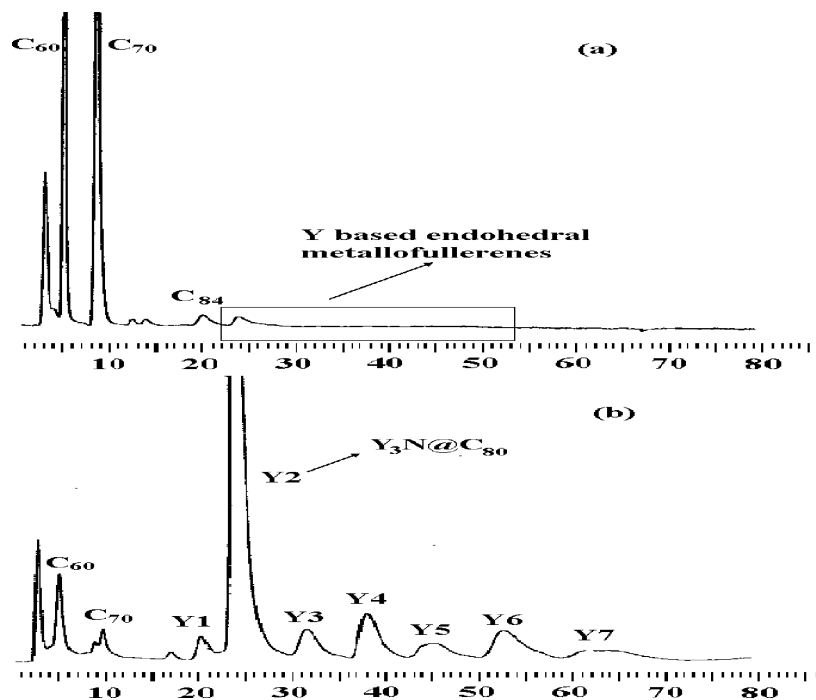
Figure 1. HPLC chromatograms of (a) the toluene extract from the raw soot and (b) the eluent from the CPDE-MPR column (both chromatograms were obtained on a 4.6 × 250 mm 5PBB column with λ = 390 nm, a flow rate of 2.0 mL/min, and toluene as the eluent at 25 °C).

stage HPLC. The first stage was carried out on a 5PBB column (4.6 × 250 mm). The different fractions (Y1−Y7) from this 5PBB column were collected and further separated with a 5PYE column (10 × 250 mm). The flow rate for both stages was 2.0 mL/min, and the detection wavelength was 390 nm. The HPLC system used an Acure series III pump and 757 absorbance detector (Applied Biosystems).

Characterization of $Y_3N@C_{2n}$. ^{13}C and ^{89}Y NMR spectroscopic measurements (150 and 29.4 MHz, respectively) on all of the samples were performed on a Bruker Avance spectrometer (600 MHz, ^1H). The samples were dissolved in carbon disulfide solution (1,2 dichlorobenzene for ^{89}Y NMR) with chromium tris(acetylacetonate), $Cr(acac)_3$, as the relaxation agent and acetone-d_6 (1,2-dichlorobenzene-d_4 for ^{89}Y NMR) as the internal lock at 25 °C. Mass spectrometry was performed on a Kratos Analytical Kompact SEQ MALDI−TOF mass spectrometer.

Computational Studies. Density functional theory (DFT) computations were performed using the Gaussian 03 program package.[53] All of the molecules were geometry optimized at the UB3LYP level with a DZVP basis set for yttrium atoms and a 6-31G* basis set for carbon and nitrogen atoms.[54] DFT-optimized energy values were obtained starting from the X-ray crystallographic structures of the corresponding $Tb_3N@C_{2n}$ (n = 40, 42−44)[40,41] and $Gd_3N@C_{2n}$ (n = 41) EMFs.[50] The energy-minimized values and the same level of theory were used to calculate all of the ^{13}C NMR chemical shifts.[54]

Results and Discussion

Preparation and Purification. The yttrium TNT EMFs $Y_3N@C_{2n}$ (n = 40−44) were prepared in a Krätschmer−Huffman

(53) Frisch, M. J.; et al. *Gaussian 03*; Gaussian, Inc.: Wallingford, CT, 2004.
(54) Zuo, T.; Xu, L.; Beavers, C. M.; Olmstead, M. M.; Fu, W. J.; Crawford, T. D.; Balch, A. L.; Dorn, H. C. *J. Am. Chem. Soc.* **2008**, *130*, 12992–12997.
(55) Diederich, F.; Whetten, R. L. *Acc. Chem. Res.* **1992**, *25*, 119–126.
(56) Johnson, R. D.; Meijer, G.; Bethune, D. S. *J. Am. Chem. Soc.* **1990**, *112*, 8983–8984.
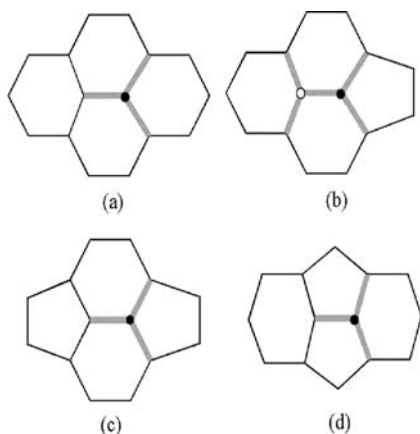
generator by vaporizing composite graphite rods containing a mixture Y_2O_3, graphite powder, and metallic Cu. The HPLC chromatogram from the toluene extract of the collected soot is shown in Figure 1a. The trace indicates that the most abundant fullerenes in the extract were empty cages, such as C_{60}, C_{70}, and C_{84}. On the basis of the greater kinetic chemical stability of the EMFs, a CPDE-MPR column was applied as the preliminary separation, as previously described.[3,41] In the HPLC trace of the eluent from the CPDE-MPR column (Figure 1b), the dominant peak was $Y_3N@C_{80}$. As Figure 1b shows, the more reactive empty-cage fullerenes (C_{60}, C_{70} and C_{84}) were strongly attenuated, and the less reactive $Y_3N@C_{2n}$ (n = 40−44) yttrium TNT EMF family became significantly concentrated.

Seven major fractions were obtained from the chemical separation step and labeled as Y1 to Y7 (Figure 1b). These fractions were further purified using HPLC with a 5PYE column, and subsequently, pure TNT EMFs were obtained for each fraction: Y1 contained $Y_2@C_{79}N$; Y2 contained two $Y_3N@C_{80}$ isomers (I_h and D_{5h}); Y3 contained $Y_3N@C_{82}$; Y4 contained $Y_3N@C_{84}$; Y5 contained $Y_3N@C_{86}$; and Y6 contained $Y_3N@C_{88}$. The Y7 fraction contained Y_2C_{94} but could not be totally characterized because of the limited amount of sample. The $Y_2@C_{79}N$ in fraction Y1 has been described previously.[54] In a fashion similar to that for the previously reported $Tm_3N@C_{80}$ isomers (I_h and D_{5h}),[49] repeated chromatographic passes were necessary to separate the Y2 fraction into pure $Y_3N@I_h-C_{80}$ and $Y_3N@D_{5h}-C_{80}$ samples. The HPLC traces, laser desorption−time of flight (LD−TOF) mass spectra, and UV−vis spectra for the purified samples are shown in the Supporting Information.

^{13}C NMR Studies. As illustrated in Figure 2, there are several common fullerene and metallofullerene carbon cage motifs that are readily recognized with characteristic ^{13}C NMR chemical shift ranges. The first three motifs (Figure 2a−c) are commonly encountered in IPR fullerenes,[31,41,55] and the other (Figure 2d)

Figure 2. (a) Pyrene motif 6,6,6 junction; (b) corannulene motif (○) 6,6,6 and (●) 6,6,5 junctions; (c) pyracylene motif 6,6,5 junction; and (d) pentalene motif 6,5,5 junction.

is the important pentalene motif found in certain non-IPR metallofullerenes, which usually exhibits highly deshielded resonances at 155−165 ppm.[33,34,40,50,51] For example, the pyracylene 6,6,5 carbon site is identified with the unique fullerene I_h-C_{60}, which has a single ^{13}C resonance at 142.5 ppm.[56] In contrast, the pyrene motif, specifically the 6,6,6 junction carbons, are typically more shielded ^{13}C resonances in the range of 130−138 ppm, as observed for the belt carbons of D_{5h}-C_{70} (130.9 ppm).[57]

$Y_3N@C_{80}$ Isomers. There are a total of 31 917 non-IPR isomers for the C_{80} cage, but only seven isomers obey the IPR. Of the seven IPR isomers for the C_{80} cage, only the I_h isomer yields a ^{13}C NMR spectrum containing two lines with a 3:1 ratio. An initial observation for the $M_3N@I_h$-C_{80} family is the relatively small perturbation of the ^{13}C NMR shifts as a function of size and metal differences of the $(M_3N)^{6+}$ clusters. This has been illustrated for several diamagnetic $Sc_3N@I_h$-C_{80}[58] and $Lu_3N@I_h$-C_{80} cages[21] as well as the mixed clusters $Lu_2YN@C_{80}$ and $LuY_2N@C_{80}$, as previously reported.[59] In the cases cited above, the I_h-C_{80} cage with the corannulene-type motif exhibits ^{13}C NMR shifts for the 6,6,5 and 6,6,6 junctions with corresponding ranges of 142.8−144.7 and 135.9−138.2 ppm. These relatively small shift ranges even include the weakly paramagnetic $CeSc_2N@C_{80}$ system.[60] The ^{13}C NMR spectrum for $Y_3N@I_h$-C_{80} (Figure 3b) supports an electronic distribution of $(Y_3N)^{6+}@(C_{80})^{6-}$ with a nearly spherical charge distribution over the fullerene cage resulting from the corannulene-type carbon atoms (intersection of three hexagons, $\delta = 138.2$ ppm) and the pyrene-type carbon atoms (intersection of a pentagon and two hexagons, $\delta = 144.6$ ppm). These resonances are similar to those of $Sc_3N@I_h$-C_{80} (137.24 and 144.57 ppm)[58] and $Lu_3N@I_h$-C_{80} (137.4 and 144.0 ppm).[21] The ^{13}C NMR spectrum at ambient temperature also confirms isotropic motional averaging of the Y_3N cluster inside the I_h cage and is consistent with the [89]Y
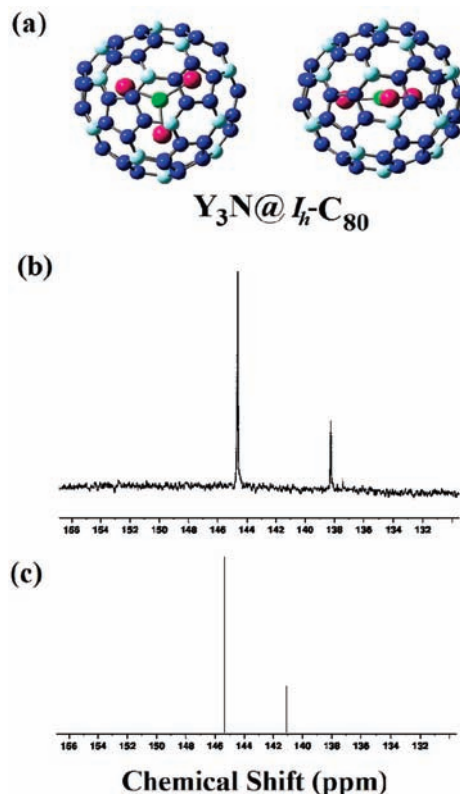

Figure 3. (a) Structure of $Y_3N@I_h$-C_{80}. (b) ^{13}C NMR spectrum of $Y_3N@I_h$-C_{80} [in CS_2 with 5 mg of $Cr(acac)_3$ relaxant, acetone-d_6 lock, 64 000 scans, 25 °C], showing the 1 × 60, 1 × 20 pattern (number of NMR lines × relative intensity). The chemical shifts for the two lines are 144.62 and 138.24 ppm. (c) Calculated ^{13}C NMR spectrum of $Y_3N@I_h$-C_{80}.

NMR results (see below). This description is supported by the computational study, but the internal rotational barrier is significantly greater for the larger $(Y_3N)^{6+}$ cluster in comparison with the smaller $(Sc_3N)^{6+}$ cluster.[61,62] The calculated ^{13}C NMR spectrum at ambient temperature (Figure 3c) also confirms motional averaging of the Y_3N cluster inside the I_h cage. The computed values are within 2−3 ppm of the experimental values but more deshielded in each case.

As previously indicated, it has been established that there are two isomers of $Sc_3N@C_{80}$ (I_h and D_{5h}, both obeying the IPR) that have been isolated and characterized.[31,58] The D_{5h} isomer also has also been characterized for other $M_3N@C_{80}$ systems, such as $Tm_3N@D_{5h}$-C_{80}[49] and $Tb_3N@D_{5h}$-C_{80}.[41] A similar situation holds for the $(Y_3N)^{6+}$ cluster, as shown by the ^{13}C NMR spectrum of the purified $Y_3N@D_{5h}$-C_{80} isomer (Figure 4b), which contains six spectral lines with the intensity ratios 1:2:2:1:1:1. As expected for $Y_3N@D_{5h}$-C_{80}, the data closely match the ^{13}C NMR data reported for other $M_3N@D_{5h}$-C_{80} isomers and do not significantly deviate as a function of the metal from the data for the $(M_3N)^{6+}$ (M = Lu, Sc) clusters.[31,32] However, the corannulene-type 6,6,5 carbon atoms (**a** in Figure 4a) are significantly deshielded relative to those for the $Y_3N@I_h$-C_{80} isomer ($\delta = 149.63$ vs 144.62 ppm). In addition, the computed value (Figure 4c) is within ∼1 ppm of the experimental value. Although a definitive assignment is not possible for all of the signals for the $Y_3N@D_{5h}$-C_{80} isomer, there appears to be good agreement between the experimental and computa-

(57) Ajie, H.; Alvarez, M. M.; Anz, S. J.; Beck, R. D.; Diederich, F.; Fostiropoulos, K.; Huffman, D. R.; Krätschmer, W.; Rubin, Y.; Schriver, K. E.; Sensharma, D.; Whetten, R. L. *J. Phys. Chem.* **1990**, *94*, 8630–8633.
(58) Stevenson, S.; Rice, G.; Glass, T.; Harich, K.; Cromer, F.; Jordan, M. R.; Craft, J.; Hadju, E.; Bible, R.; Olmstead, M. M.; Maitra, K.; Fisher, A. J.; Balch, A. L.; Dorn, H. C. *Nature* **1999**, *401*, 55–57.
(59) Yang, S. F.; Popov, A.; Dunsch, L. *Angew. Chem., Int. Ed.* **2008**, *47*, 8196–8200.
(60) Wang, X.; Zuo, T.; Olmstead, M. M.; Duchamp, J. C.; Glass, T. E.; Cromer, F.; Balch, A.; Dorn, H. C. *J. Am. Chem. Soc.* **2006**, *128*, 8884–8889.

(61) Popov, A. A.; Dunsch, L. *J. Am. Chem. Soc.* **2008**, *130*, 17726–17742.
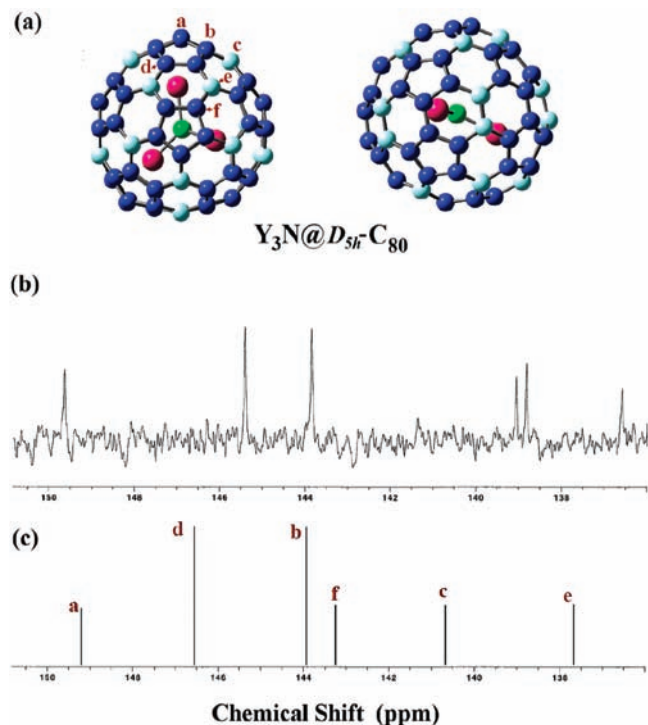(62) Gan, L.-H.; Yuan, R. *ChemPhysChem* **2006**, *7*, 1306–1310.

Figure 4. (a) Structure of $Y_3N@D_{5h}$-C_{80}. (b) ^{13}C NMR spectrum of $Y_3N@D_{5h}$-C_{80} [in CS_2 with 12 mg of $Cr(acac)_3$ relaxant, acetone-d_6 lock, 75 000 scans, 25 °C], showing the 2 × 20, 4 × 10 pattern (number of NMR lines × relative intensity). The chemical shifts for the six lines are 149.63, 145.40 (double intensity), 143.85 (double intensity), 139.06, 138.82, and 136.58 ppm. (c) Calculated ^{13}C NMR spectrum of $Y_3N@D_{5h}$-C_{80}.

tional values for **b** and **d**. On the other hand, the pyracylene 6,6,5 carbon site **f** (computed δ value: 143.3 ppm) is not definitively assignable, but it must be one of the three most shielded resonances (139.06, 138.82, and 136.58 ppm) with intensity ratios of 1:1:1. These values indicate significantly more shielding than for typical pyracylene 6,6,5 carbon sites, such as those in I_h-C_{60} (δ = 142.5 ppm)[56] or the end-cap pyracylene carbons in D_{5h}-C_{70} (δ = 150.7 ppm).[57] The corresponding deshielding and shielding effects observed for carbon sites **a** and **f**, respectively, could result from restricted motion of the $(Y_3N)^{6+}$ cluster in the horizontal plane of the D_{5h} isomer. These results deserve further study, but the current results clearly illustrate the importance of the position and motional process of the internal $(M_3N)^{6+}$ cluster in determining the ^{13}C NMR chemical shifts.

$Y_3N@C_{82}$. It was predicted that $M_3N@C_{82}$ is a non-IPR structure because of the small gap in the molecular orbital energy in the hexaanion of the empty C_{82} cage.[63] Popov and Dunsch suggested on the basis of computational approaches that the most plausible isomers for the TNT EMFs with C_{82} cages are $M_3N@C_{2v}$(39705)-C_{82} and $M_3N@C_s$(39663)-C_{82}.[64] Remarkably, Echegoyen and Balch[50] recently reported the egg-shaped structure of $Gd_3N@C_s$(39663)-C_{82} obtained using single-crystal X-ray diffraction, consistent with the earlier predictions of Popov and Dunsch.

There are 39 709 possible non-IPR isomeric structures, and among them are 27 isomers with C_s symmetry. The ^{13}C NMR spectrum of $Y_3N@C_{82}$ (Figure 5b) exhibits 45 lines, 37 with
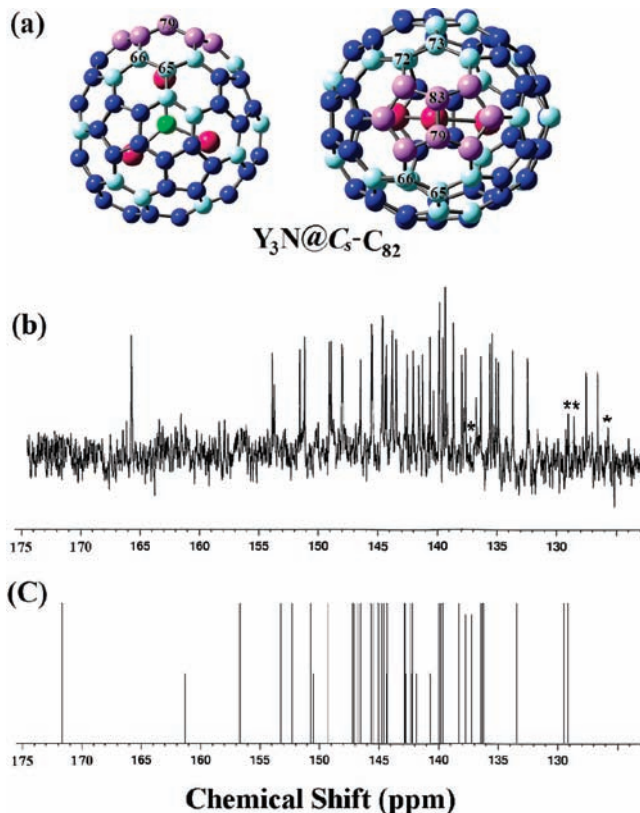
(63) Campanera, J. M.; Bo, C.; Poblet, J. M. *Angew. Chem., Int. Ed.* **2005**, *44*, 7230–7233.
(64) Popov, A. A.; Dunsch, L. *J. Am. Chem. Soc.* **2007**, *129*, 11835–11849.
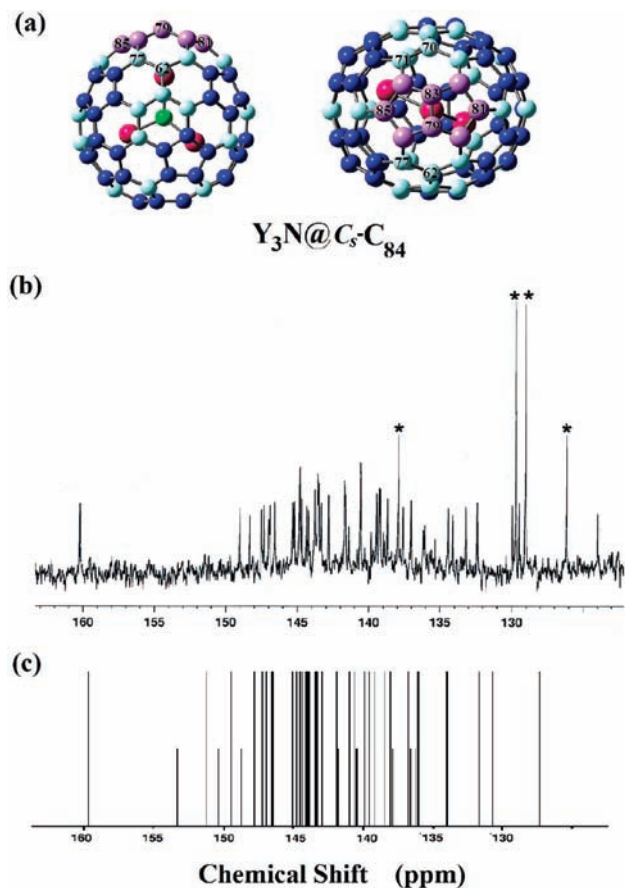
Figure 5. (a) Structure of $Y_3N@C_s$(39663)-C_{82}. (b) ^{13}C NMR spectrum of $Y_3N@C_s$(39663)-C_{82} [in CS_2 with 10 mg of $Cr(acac)_3$ relaxant, acetone-d_6 lock, 120 000 scans, 25 °C], showing the 37 × 2, 8 × 1 pattern (number of NMR lines × relative intensity). The chemical shifts for the 45 lines are 165.69, 153.84, 153.70 (half-intensity), 151.51, 151.14, 149.03, 148.89, 148.03, 147.93, 146.43, 145.53, 145.45, 144.59, 145.55, 144.37 (half-intensity), 144.28, 143.81 (half-intensity), 143.77, 143.43, 143.41 (half-intensity), 142.53, 142.01, 141.53, 141.25, 140.61, 140.30 (half-intensity), 139.87, 139.82, 139.52, 139.34, 139.17 (half-intensity), 138.66, 137.96, 137.77 (half-intensity), 137.63, 136.76 (half-intensity), 136.35, 135.58, 135.42, 135.07, 134.89, 133.67, 132.40, 127.52, and 126.55 ppm. The * labels indicate signals from the residual toluene in the sample. (c) Calculated ^{13}C NMR spectrum of $Y_3N@C_s$(39663)-C_{82}.

full intensity and 8 with half intensity (37 × 2, 8 × 1 pattern), consistent with a C_s-symmetric structure. The observed spectral line at 165.7 ppm (DFT prediction: 171.7 ppm) is also consistent with the pentalene carbons (C79, C83) for this non-IPR structure. These carbons are significantly more deshielded than most pentalene carbons reported to date, presumably because of the greater strain of the pentalene motif in this case.[33,35] The half-intensity signals at 153.7, 144.37, 143.87, and 143.81 are consistent with the four pyracylene 6,6,5 junction carbons in the symmetry plane of the C_s(39663)-C_{82} cage. Assuming that the two half-intensity corannulene 6,6,5 carbons are the signals at 140.3 and 139.7 ppm leaves two half-intensity 6,6,6 pyrene signals at 137.77 and 136.76 ppm. The DFT-computed values for these half-intensity signals are typically 3−5 ppm more deshielded than the experimental values. There are 11 pyrene-type 6,6,6 carbons for the C_s(39663)-C_{82} structure, tentatively assigned to the 11 (2 × 1) ^{13}C NMR chemical signals below 138 ppm. Especially interesting are the two signals (127.52 and 126.55 ppm) from the highly shielded pyrene 6,6,6 carbons that are spatially located over the Y atom complexed to the pentalene site (C65, C66, C72, and C73, as shown in Figure 5a). These two signals appear to be 2−3 ppm more shielded, but are clearly identified by the DFT results. Although a ^{13}C NMR INAD-

Figure 6. (a) Structure of Y$_3$N@C_s(51365)-C$_{84}$. (b) ^{13}C NMR spectrum of Y$_3$N@C_s(51365)-C$_{84}$ [in CS$_2$ with 10 mg of Cr(acac)$_3$ relaxant, acetone-d_6 lock, 106 000 scans, 25 °C], showing the 2 × 37, 1 × 10 pattern (number of NMR lines × relative intensity). The chemical shifts for the 47 lines are 160.24, 149.50 (half-intensity), 149.00, 148.32, 147.49, 147.33, 146.98 (half-intensity), 146.91, 146.59, 145.31, 145.21, 144.86, 144.83, 144.7, 144.37, 144.23, 143.78, 143.61, 143.56, 143.5, 143.34, 142.81, 141.68, 141.63, 141.38 (half-intensity), 140.58, 139.86 (half-intensity), 139.46, 139.25, 139.20, 138.96 (half-intensity), 138.86 (half-intensity), 138.70, 137.96, 137.59, 137.02, 136.18 (half-intensity), 136.12 (half-intensity), 135.35 (half-intensity), 134.44, 134.12, 133.28 (half-intensity), 133.18, 132.39, 129.96, 129.49, and 124.01 ppm. The * labels indicate signals from the residual toluene in the sample. (c) Calculated ^{13}C NMR spectrum of Y$_3$N@C_s(51365)-C$_{84}$.

EQUATE study is necessary to completely define the carbon−carbon connectivity and corresponding structure, the current study confirms that the ^{13}C NMR spectrum for Y$_3$N@C$_{82}$ is consistent with the cage reported for Gd$_3$N@C_s(39663)-C$_{82}$.[50]

Y$_3$N@C$_{84}$. Although there are 51 568 non-IPR and 24 IPR structures for C$_{84}$, the most abundant M$_3$N@C$_{84}$ (M = Tb, Tm, Gd) isomer was confirmed by an X-ray diffraction study to be an egg-shaped structure with non-IPR C_s symmetry.[40,51] The C$_{84}$ cage in M$_3$N@C_s(51365)-C$_{84}$ (M = Tb, Tm, Gd) closely resembles the cage of Gd$_3$N@C_s(39663)-C$_{82}$. The cage has a single pentalene, and a symmetry plane bisects this motif (Figure 6a).

Figure 6b, c shows the high-resolution experimental and calculated ^{13}C NMR spectra of the Y$_3$N@C$_{84}$. The experimental spectrum consists of 47 lines, 37 with full intensity and 10 with half intensity (37 × 2, 10 × 1 pattern), consistent with a C_s-symmetric structure. The wide range of chemical shifts is 124.01−160.24 ppm. There is one highly deshielded resonance at 160.24 ppm, confirming the presence of the pentalene motif (carbons C79, C83) for this non-IPR structure. The theoretical ^{13}C NMR chemical shift range, 127.39−159.71 ppm, is in
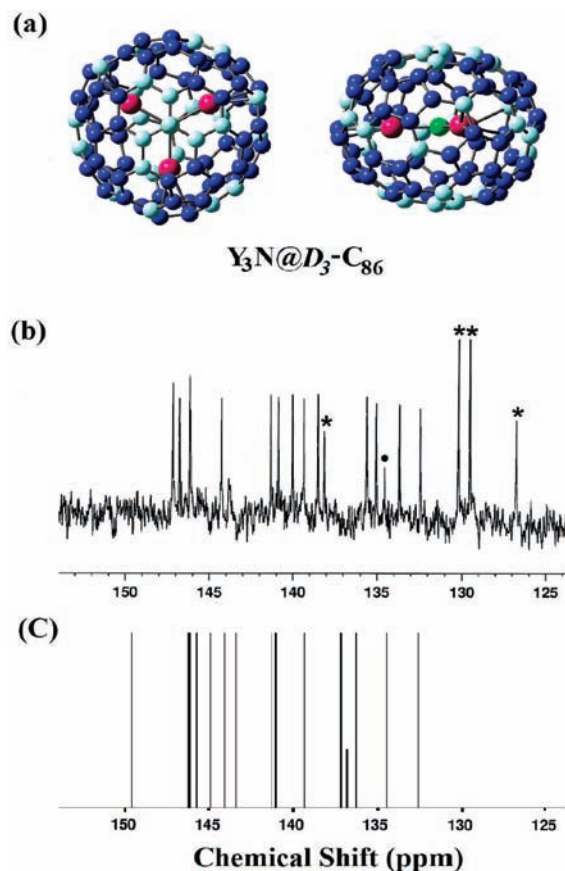

Figure 7. (a) Structure of Y$_3$N@D_3-C$_{86}$. (b) ^{13}C NMR spectrum of Y$_3$N@D_3-C$_{86}$ [in CS$_2$ with 10 mg of Cr(acac)$_3$ relaxant, acetone-d_6 lock, 108 000 scans, 25 °C], showing the 14 × 6, 1 × 2 pattern (number of NMR lines × relative intensity). The chemical shifts for the 15 lines are 146.84, 146.42, 145.78, 145.72, 143.81, 140.79, 140.32, 139.42, 138.71, 137.87, 134.89, 134.31, 133.81 (one-third intensity), 132.92, and 131.60 ppm. The * labels indicate signals from the residual toluene in the sample. The • label shows the signal with one-third intensity. (c) Calculated ^{13}C NMR spectrum of Y$_3$N@D_3-C$_{86}$.

excellent agreement with the experimental spectrum. Two nonequivalent 6,6,5 pyracylene carbons (C81, C85) can be assigned to the experimental half-intensity peaks at 149.5 and 146.98 ppm. These values are significantly more deshielded than the corresponding DFT-computed values of 153.36 and 150.31 ppm. One isolated peak in the downfield region of the spectrum is due to pyrene carbon 6,6,6 signals (124.01 ppm), which matches the DFT-calculated spectrum. Similar to the case of the Y$_3$N@C_s(39663)-C$_{82}$ isomer, this corresponds to the highly shielded pyrene carbon signals (C62, C70) that are spatially located over the Y atom complexed to the pentalene site. To summarize, the ^{13}C NMR spectrum for Y$_3$N@C_s(51365)-C$_{84}$ is consistent with the carbon cage previously reported for the corresponding terbium isomer.

Y$_3$N@C$_{86}$. The ^{13}C NMR spectrum for Y$_3$N@C$_{86}$ (Figure 7b) exhibits a total of only 15 lines (14 full-intensity peaks and a peak with one-third intensity) with a relatively narrow range of only ∼15 ppm, in sharp contrast with the much wider spectral ranges for Y$_3$N@C$_{82}$ and Y$_3$N@C$_{84}$. The ^{13}C NMR spectrum of Y$_3$N@C$_{86}$ suggests an IPR-allowed isomer because of the absence of a ^{13}C NMR signal at >155 ppm that would be characteristic of a pentalene motif. There are 19 IPR-allowed C$_{86}$ isomers, of which two neutral isomers with C_2 and C_s symmetry are reported to be stable on the basis of experimental

and computational studies.[66] However, another TNT EMF, $Tb_3N@D_3(19)$-C_{86}, exhibits D_3 carbon-cage symmetry, as determined by previous single-crystal X-ray diffraction studies.[41] This result is completely consistent with the 15 ^{13}C NMR signals observed for $Y_3N@C_{86}$. In addition, none of the other IPR-allowed structures would exhibit fewer than 24 lines because these remaining structures all have lower symmetry.[67] The ^{13}C NMR resonances for the carbons along the D_3 symmetry axis (2×1, one-third intensity) are easily identified (133.9 ppm) and in excellent agreement with the DFT prediction of 136.81 ppm. In addition, there are six pyrene-type 6,6,6 carbons with chemical shifts in the range 131.6–138.7 ppm, in reasonable agreement with the six DFT-predicted values in the 132.5–141.1 ppm range.

[89]Y NMR Study. As previously indicated, the [89]Y nuclide ($I = 1/2$) is 100% abundant, but [89]Y NMR studies have been hampered by the low magnetogyric ratio and corresponding long spin–lattice (T_1) relaxation times. Although high magnetic fields and long scan times were required in the current study, this could be alleviated in future studies by using higher fields and dynamic nuclear polarization approaches.[52] The low sensitivity precluded us from obtaining [89]Y NMR data for samples with limited quantities [e.g., $Y_3N@C_s(39663)$-C_{82}]. However, in the case of the internal yttrium cluster in the icosahedral C_{80} cage, we observed a single sharp resonance line for $Y_3N@I_h$-C_{80} at 191.63 ppm [computed value: 237.64 ppm (see the Supporting Information)], consistent with isotropic rotation of the $(Y_3N)^{6+}$ cluster at ambient temperatures. This is consistent with the [45]Sc NMR data for $Sc_3N@I_h$-C_{80} reported previously.[58] In the case of some restricted motion of the clusters, as represented by the $Y_3N@D_3$-C_{86} cage, the [89]Y NMR signal (Figure 8) for the $Y_3N@D_3$-C_{86} sample is more strongly shielded (62.65 vs the computed value of 131.79 ppm).

As expected for $Y_3N@C_s(51365)$-C_{84}, the coordination of one Y atom with the pentalene motif (Figure 6a) and the more restricted internal cage surface should yield three different electronic environments for the yttrium atoms of the $(Y_3N)^{6+}$ cluster at ambient temperature. As shown in Figure 8d, three [89]Y NMR signals are observed at 104.32, 65.33, and −19.53 ppm (relative to external YCl_3). These values are consistent with the computed values of 146.84, 102.08, and 14.95 ppm, assuming a constant error in the reference of 35−40 ppm (see the Supporting Information). In previous solution [89]Y NMR studies, it has been observed that there is a strong shielding effect for Y^{3+} ions complexed to pentamethylcyclopentadienyl moieties. White and Hanusa[65] have reported that this [89]Y chemical shielding effect is ~100 ppm per cyclopentadienyl unit in organometallic complexes. On the basis of this additivity effect and our computational result (14.95 ppm), we tentatively assign the [89]Y NMR signal at −19.53 ppm to the Y atom complexed to the pentalene moiety in $Y_3N@C_s(51365)$-C_{84}.

The surprising results above are supported by the [89]Y NMR shielding DFT computational study (at the UB3LYP/DZVP level for yttrium), as illustrated in Figure S5 in the Supporting Information. It should be noted that in all cases, the calculated shielding values are for the most stable cluster and cage conformation. The current study utilizes $[Y(H_2O)_8]^{3+}$ as the reference; this same reference was employed in the earlier study of organometallic complexes by White and Hanusa.[65] It is expected that larger bulk magnetic susceptibility differences are
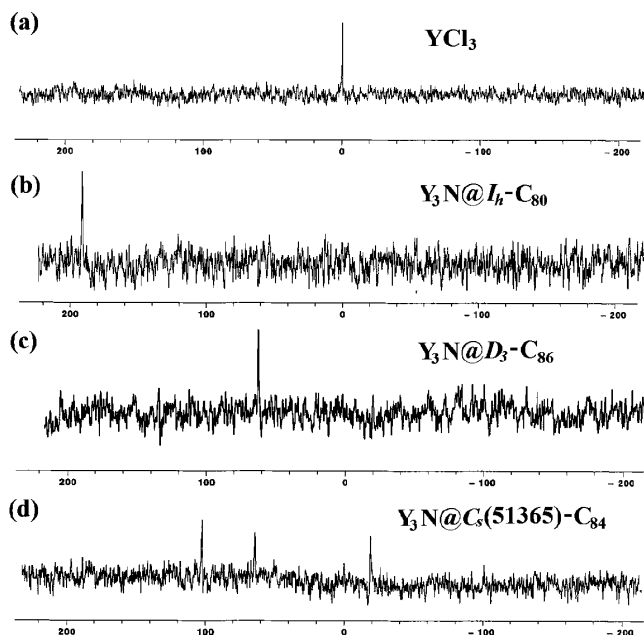

Figure 8. [89]Y NMR spectra at 25 °C: (a) YCl_3 (in D_2O, 32 scans; external reference). (b) $Y_3N@I_h$-C_{80} [in dichlorobenzene with 20 mg of $Cr(acac)_3$ relaxant, 1,2-dichlorobenzene-d_4 lock, 51 520 scans]. The chemical shift for the one line is 191.63 ppm. (c) $Y_3N@D_3$-C_{86} [in dichlorobenzene with 30 mg of $Cr(acac)_3$ relaxant, 1,2-dichlorobenzene-d_4 lock, 51 920 scans]. The chemical shift for the one line is 62.65 ppm. (d) $Y_3N@C_s(51365)$-C_{84} [in 1,2-dichlorobenzene with 20 mg of $Cr(acac)_3$ relaxant, 1,2-dichloroben-zene-d_4 lock, 41 200 scans]. The chemical shifts for the three lines are 104.32, 65.33, and −19.53 ppm.

possible in comparison with the less polar 1,2-dichlorobenzene solvent employed in the present study. A correlation coefficient of 0.95 was obtained, and the calculated and experimental values exhibit average deviations of less than 12.4 ppm (see Figure S5). Clearly, a more detailed computational chemical shift study with other conformations for the cluster could provide additional details of the cluster motion. Nevertheless, a key finding of the current study is the sensitivity of the [89]Y NMR chemical shift parameter to subtle changes in the electronic environment at each yttrium nuclide in the $(Y_3N)^{6+}$ cluster (a range of over 200 ppm), and these results clearly demonstrate that [89]Y NMR spectroscopy will evolve as a powerful tool for understanding motional processes of yttrium clusters in EMFs and other organometallics.

Conclusion

In summary, a series of yttrium-based TNT EMFs have been isolated, and the carbon cages have been characterized by experimental and computational ^{13}C NMR spectroscopy. These structures include $Y_3N@I_h$-C_{80}, $Y_3@D_{5h}$-C_{80}, $Y_3N@C_s(39663)$-C_{82}, $Y_3N@C_s(51365)$-C_{84}, and $Y_3N@D_3$-C_{86}. One general observation for the $M_3N@C_{80}$ family is the relatively small perturbation of the ^{13}C NMR shifts as a function of size and metal differences in the $(M_3N)^{6+}$ clusters. The first [89]Y NMR results have been obtained for $Y_3N@I_h$-C_{80}, $Y_3N@C_s(51365)$-C_{84}, and $Y_3N@D_3$-C_{86}, and these results suggest that the [89]Y NMR shift parameter is very sensitive to subtle changes in the carbon cage. The [89]Y and ^{13}C NMR spectra at ambient temperature also confirm that isotropic motional averaging of the Y_3N cluster occurs inside certain cages (e.g., $Y_3N@I_h$-C_{80}) but is certainly restricted in other cases [e.g., $Y_3N@C_s(51365)$-C_{84}]. The DFT computational approach provides good agreement with the experimental [13]C

(65) White, R. E.; Hanusa, T. P. *Organometallics* **2006**, *25*, 5621–5630.
(66) Sun, G.; Kertesz, M. *Chem. Phys.* **2002**, *276*, 107–114.
(67) Fowler, P. W.; Manolopoulos, D. E. *An Atlas of Fullerenes*; Clarendon Press: Oxford, U.K., 1995.

results. Interestingly, the level of agreement appears to improve for cases where the $(Y_3N)^{6+}$ cluster is more restricted [e.g., $Y_3N@C_s(39663)\text{-}C_{82}$ and $Y_3N@C_s(51365)\text{-}C_{84}$]. This is supported by the improved correlation between the DFT-computed and experimental results for the latter restricted systems (see the Supporting Information). In summary, this ^{13}C and ^{89}Y NMR study confirms the unique role of the trimetallic nitride $(Y_3N)^{6+}$ cluster template in forming a limited number of high-symmetry isomers in the $Y_3N@C_{2n}$ ($n = 40-43$) family.

Supporting Information Available: Complete ref 53 and Figures S1−S10. This material is available free of charge via the Internet at http://pubs.acs.org.

JA902286V